Maximizing phononic band gaps in piezocomposite materials by means of topology optimization

Sandro L. Vatanabe
Department of Mechatronics and Mechanical Systems Engineering, Polytechnic School of University of São Paulo, SP 05508-900, Brazil

Glaucio H. Paulino
Newmark Laboratory, Department of Civil and Environmental Engineering and Department of Mechanical Science and Engineering, University of Illinois at Urbana-Champaign, Urbana, Illinois 61801

Emílio C. N. Silva[a)]
Department of Mechatronics and Mechanical Systems Engineering, Polytechnic School of University of São Paulo, SP 05508-900, Brazil

(Received 13 September 2013; revised 15 May 2014; accepted 21 June 2014)

Phononic crystals (PCs) can exhibit phononic band gaps within which sound and vibrations at certain frequencies do not propagate. In fact, PCs with large band gaps are of great interest for many applications, such as transducers, elastic/acoustic filters, noise control, and vibration shields. Previous work in the field concentrated on PCs made of elastic isotropic materials; however, band gaps can be enlarged by using non-isotropic materials, such as piezoelectric materials. Because the main property of PCs is the presence of band gaps, one possible way to design microstructures that have a desired band gap is through topology optimization. Thus in this work, the main objective is to maximize the width of absolute elastic wave band gaps in piezocomposite materials designed by means of topology optimization. For band gap calculation, the finite element analysis is implemented with Bloch–Floquet theory to solve the dynamic behavior of two-dimensional piezocomposite unit cells. Higher order frequency branches are investigated. The results demonstrate that tunable phononic band gaps in piezocomposite materials can be designed by means of the present methodology. © *2014 Acoustical Society of America*. [http://dx.doi.org/10.1121/1.4887456]

PACS number(s): 43.20.Gp, 43.40.Sk, 43.20.El, 43.40.Fz [ANN] Pages: 494–501

I. INTRODUCTION AND MOTIVATION

Piezoelectric materials are frequently used in engineering applications, especially in the aeronautical and aerospace engineering. Many of the piezoelectric components that are extensively employed in intelligent materials and structures exhibit periodicity.[1] Acoustic or elastic composite materials, called phononic crystals (PCs), can exhibit ranges of frequencies, known as stopbands or band gaps, over which all incident waves are effectively attenuated. This attenuation phenomenon is attributed to a mechanism of destructive interferences within the scattered wave field.[2] Due to its potential range of applications, several computational methods have been developed to compute band gaps properties of PCs.[3] The existence of band gaps suggests that it may be used as filters, as transducers, for creation of vibration-free environments, and for energy harvesting applications.[4] Thus it is essential to design a microstructure that possesses a desired band gap configuration. The design of PCs with tunable band gaps is an interesting and challenging problem. Substantial research has been done to enlarge the width of band gaps[5,6] that shows that the width of band gaps is determined by the contrast of elastic constants, the filling volume fraction, and the lattice of the constructed elements. Previous studies on dispersive composite materials have focused on elastic periodic structures,[7–12] and not much work has been done using piezocomposite structures.[13–15] Previous investigations of wave propagation in two-dimensional models have considered the piezoelectric polarization fixed in the z direction (normal to the surface). Wilm *et al.*[13] implemented a three-dimensional model based on a plane wave expansion of the generalized acoustic fields for general piezoelectric-based composite materials. Hou *et al.*[14] investigated the elastic band structure of a two-dimensional phononic crystal containing piezoelectric material by means of the plane-wave-expansion method. Numerical results show that for a large filling fraction, the full band gap of this kind of system is enlarged by considering the piezoelectric effect; however, for a small filling fraction, the influence of the piezoelectric effect is so small that it can be neglected. Wilm *et al.*[15] investigated not only waves propagating in the symmetry plane of piezocomposites but also waves propagating with a nonzero angle of incidence with this plane. The main conclusion is that by locating the thickness mode in band gaps allows minimization of coupling with parasitic modes such as lateral modes, or even propagation of Lamb waves in phased array or excitation of plate modes.

Because the main property of PCs is the presence of band gaps, it is essential to design microstructures with band gaps as large as possible. However, each kind of application requires a distinct frequency band gap, and thus, a possible

[a)]Author to whom correspondence should be addressed. Electronic mail: ecnsilva@usp.br

way to design structures with a desired band gap is by means of the topology optimization method (TOM).[16] Such a method consists of seeking an optimal structural topology design by determining which points of space should be solid and which points should be void (i.e., no material) inside a given domain.[17] Sigmund and Jensen[5] applied topology optimization to design periodic materials and structures exhibiting phononic band gaps to either minimize the structural response along boundaries (wave damping) or maximize the response at certain boundary locations (waveguiding). Halkjær *et al.*[18] maximized phononic band gaps for infinite, periodic beam structures modeled by Timoshenko beam theory, for infinite periodic, thick and moderately thick plates, and for finite thick plates. Halkjær *et al.*[19] maximized the band gap size for bending waves in a Mindlin plate, and they constructed a finite periodic plate using a number of the optimized base cells in a postprocessed version. Rupp *et al.*[20] applied the TOM to design two- and three-dimensional phononic (elastic) materials, focusing on surface wave filters and waveguides.

In this work, the goal is to design two-dimensional piezocomposite materials that maximize the relative band gap size between frequencies j and $j+1$, i.e., maximize the lowest value of the upper bound of the band gap and minimize the maximum value of the lower bound of the band gap, by using topology optimization. The modeling combines the finite element method (FEM) and Bloch–Floquet theory.

This paper is organized as follows, in Sec. II, the piezoelectric constitutive equations are described. In Sec. III, the theoretical formulation for band gap modeling is given with emphasis on the aspects related to the periodicity. For the sake of simplicity, only the two-dimensional mathematical model is described. In Sec. IV, the TOM applied to phononic piezocomposite material design is presented. In Sec. V, the numerical implementation is detailed. In Sec. VI, optimized material designs are developed aiming at maximizing band gaps of different orders. Finally, in Sec. VII, some conclusions are inferred.

II. PIEZOELECTRIC CONSTITUTIVE EQUATIONS

The stress-charge form of the constitutive relation for piezoelectric media are given by[21,22]

$$\begin{aligned} \mathbf{T} &= \mathbf{c}^E\mathbf{S} - \mathbf{e}\mathbf{E} \\ \mathbf{D} &= \mathbf{e}^t\mathbf{S} + \boldsymbol{\varepsilon}^S\mathbf{E}, \end{aligned} \tag{1}$$

where $\mathbf{T}$, $\mathbf{S}$, $\mathbf{D}$, and $\mathbf{E}$ are, respectively, the mechanical stress tensor, the mechanical strain tensor, the electric charge vector, and the electric field vector. The term $\mathbf{c}^E$ represents the elastic stiffness tensor, which is evaluated at a constant electric field. Terms $\mathbf{e}$ and $\boldsymbol{\varepsilon}^S$ are, respectively, the piezoelectric tensor, and the dielectric tensor evaluated at constant strain.

In this work, a bidimensional model is considered. By convention, the polarization axis of the piezoelectric material is considered in the vertical direction. Moreover, a plane-strain assumption is considered for modeling two-dimensional microstructures. Therefore, by assuming that the model is in the plane 1–3 (x-z) (y is the normal direction) and that the piezoelectric material employed to build the piezocomposite belongs to the hexagonal 6 mm class, we obtain the correspondent plane-strain properties by considering $\varepsilon_y = 0$ and $E_y = 0$ in Eq. (1) and rewriting them by using only the terms ε_i, T_i, D_i, and E_i for $i = 1$ or 3. A plane-stress model could also be considered; however, it is less realistic than the plane-strain model for representing the composite behavior, which is assumed to have an infinite length in the y direction (for the two-dimensional case).

III. FORMULATION

As indicated previously, the model adopted in this work is a two-dimensional infinite periodic medium under plane strain conditions. Figure 1(a) shows an example of a unit cell with a cylindrical inclusion in a matrix of different material. Due to periodicity of the material, the lines A_1 and A_2, parallel to the y axis, and the lines B_1 and B_2, parallel to the x axis, limit the unit cell, which is of length $2d_a$ wide in the x direction and $2d_b$ in the y direction. In Fig. 1(a), corners are marked by the letter C. The unit cell is excited by a monochromatic plane wave, which is characterized by a real wave vector

$$\mathbf{k} = k\cos\theta\vec{i} + k\sin\theta\vec{j}. \tag{2}$$

The magnitude k is the wavenumber (inversely proportional to the wavelength), and its direction θ is ordinarily the direction of wave propagation. Its modulus is called the wave number and is denoted by the scalar k. The direction of incidence is marked by an angle θ with respect to the positive x axis. Because the material is assumed to be periodic and infinite in the x and y directions, then any space function F agrees with the classical Bloch relation[9]

$$\begin{aligned} F(x+2d_a,\, y+2d_b) &= e^{j2d_a k\cos\theta} e^{j2d_b k\sin\theta} F(x,\, y) \\ &= e^{j\phi_a} e^{j\phi_b} F(x,\, y)\,. \end{aligned} \tag{3}$$

Figure 1(b) shows the first Brillouin zone for an orthotropic unit cell. In principle, the whole area should be searched; however, although unproven, researchers have claimed that if the scope of the analysis is the determination of band gaps, the information required can be obtained by searching points only on the boundary lines.[5] This approach is followed in the present work.

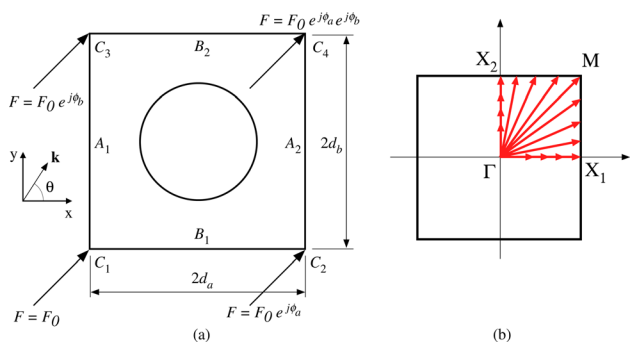

FIG. 1. (Color online) (a) Schematic description of a doubly periodic material. (b) First Brillouin zone for an orthotropic unit cell.

A. Finite element modeling of the piezocomposite unit cell

A generic numerical method, such as the finite element method (FEM), is necessary for structural analysis because structures with complex topologies are expected. Therefore the formulation of the FEM for linear piezoelectricity is utilized. Because this formulation is well developed in the literature, only a brief description will be given here.[23] The material is considered as an infinitely periodic media, and thus it is possible to reduce the finite element model to only one unit cell. This is done by applying Eq. (3) to the degrees of freedom located at the unit-cell boundaries. In the case of piezocomposite materials, there are 3 degrees of freedom at each node, which are displacements $\mathbf{U}$ (in x and y direction) and electrical potential ϕ.

The finite element equations for modeling a linear piezoelectric medium, considering time harmonic excitation, may be written as[23]

$$\left(\begin{bmatrix}\mathbf{K_{uu}} & \mathbf{K_{u\phi}}\\ \mathbf{K}^t_{\mathbf{u}\phi} & \mathbf{K}_{\phi\phi}\end{bmatrix} - \omega^2\begin{bmatrix}\mathbf{M} & 0\\ 0 & 0\end{bmatrix}\right)\begin{Bmatrix}\mathbf{U}\\ \mathbf{\Phi}\end{Bmatrix} = \left(\mathbf{K}^* - \omega^2\mathbf{M}^*\right)\mathbf{U}^* = \mathbf{0}, \tag{4}$$

where $\mathbf{M}$, $\mathbf{K_{uu}}$, $\mathbf{K_{u}}\phi$, and $\mathbf{K}_{\phi\phi}$ are the mass, stiffness, piezoelectric, and dielectric matrices, respectively, and $\mathbf{U}$ and $\mathbf{\Phi}$ denote the nodal displacement and nodal electric potential vectors, respectively.[23] Equation (4) represents the FEM model for piezoelectricity without damping effect. In all the examples in this paper, four node isoparametric elements are used with a linear interpolation along element edges.

B. Periodic boundary conditions

The application of the periodic boundary conditions implies that the phase relation of Eq. (3) between nodal values belonging to the lines A_1 and A_2, on the one hand, and between the lines B_1 and B_2, on the other hand, has to be incorporated in the matrix Eq. (4). The unit cell is divided into nine parts: The four lines A_1, A_2, B_1, and B_2, the four corners C_1, C_2, C_3, and C_4, and the inner domain I. The displacement vector $\mathbf{U}$ and electrical potential vector $\mathbf{\Phi}$ are then split into the corresponding nine parts. Using Eq. (3), we have

$$\begin{aligned}&\mathbf{U}^*_{A_2} = \mathbf{U}^*_{A_1}e^{j\varphi_a}, \quad \mathbf{U}^*_{B_2} = \mathbf{U}^*_{B_1}e^{j\varphi_b} \quad \mathbf{U}^*_{C_2} = \mathbf{U}^*_{C_1}e^{j\varphi_a},\\ &\mathbf{U}^*_{C_3} = \mathbf{U}^*_{C_1}e^{j\varphi_b}, \quad \mathbf{U}^*_{C_4} = \mathbf{U}^*_{C_1}e^{j(\varphi_a+\varphi_b)}.\end{aligned} \tag{5}$$

By defining the reduced vector $\mathbf{U}_R$ as a vector containing the nodal values of the displacement on the lines A_1 and B_1, on the C_1 corner and in the inner domain I, we use Eq. (5) to obtain a simple matrix relation between $\mathbf{U}$ and $\mathbf{U}_R$, which can be written as

$$\mathbf{U}^* = \mathbf{P}_U\mathbf{U}_R = \mathbf{P}_U\begin{bmatrix}\mathbf{U}^*_{A_1}\\ \mathbf{U}^*_{B_1}\\ \mathbf{U}^*_{C_1}\\ \mathbf{U}^*_{I}\end{bmatrix}, \tag{6}$$

where $\mathbf{P}_U$ has the same size of the stiffness matrix $\mathbf{K}^*$ and is filled by 1 at the degrees of freedom correlating the periodic boundaries and 0 at all the other locations. In terms of finite elements, this operation is the static condensation of degrees of freedom belonging to A_2, B_2, C_2, C_3, and C_4. Thus Eq. (4) can be rewritten as

$$\mathbf{P}^t_U\left(\mathbf{K}^* - \omega^2\mathbf{M}^*\right)\mathbf{P}_U\mathbf{U}_R = \left(\mathbf{K}_R - \omega^2\mathbf{M}_R\right)\mathbf{U}_R = \mathbf{0}, \tag{7}$$

where

$$\mathbf{K}_R = \mathbf{P}^t_U\mathbf{K}^*\mathbf{P}_U \text{ e } \mathbf{M}_\mathrm{R} = \mathbf{P}^\mathrm{t}_\mathrm{U}\mathbf{M}^*\mathbf{P}_\mathrm{U}. \tag{8}$$

The angular frequency ω is a periodic function of the wave vector $\mathbf{k}$. Thus the problem can be reduced to the first Brillouin zone. The dispersion curves are built by varying the wave vector $\mathbf{k}$ on the first Brillouin zone, for a given propagation direction, and solving the eigenvalue problem.

IV. TOPOLOGY OPTIMIZATION

The optimization framework considers that each finite element can assume properties of a collection of predetermined materials, and the optimization solver is responsible for defining the material distribution in the design domain. If two different materials are chosen, aluminum and epoxy, for instance, the design variables represent these materials by values equal to either one or zero, where one represents aluminum and zero, epoxy. In topology optimization, this case is known as binary (0–1) design. However, the abrupt changes of the properties of each finite element during the optimization iterations make the numerical treatment of the problem difficult, due to the discontinuities in the solution space. So, the binary (0–1) design is an ill-posed problem[16] and thus, a typical way to seek a solution consists of relaxing the problem by defining a material model that allows for intermediate (composite) property values. In this sense, the relaxation yields a continuous material design problem that no longer involves a discernible connectivity. A feasible topology solution can be obtained by applying penalization coefficients to the material model to recover the 0–1 design (and thus, a discernible connectivity), and some gradient control of material distribution, such as a filter.[16]

The design domain, in the case of material design, is the unit-cell domain. The topology optimization formulation, implemented in this work, considers a material model based on the solid isotropic material with penalization (or SIMP);[16] however, other material models could also be employed.[16] The traditional SIMP model states that at each point of the domain, the local effective property Ψ_H of the mixture is

$$\Psi_H = \rho\Psi_B + (1-\rho)\Psi_A \quad i = 1,...,N, \tag{9}$$

where Ψ_A and Ψ_B are the constituent material properties, which correspond either to the specific weight property or to the elastic ($\mathbf{c}^E$), piezoelectric ($\mathbf{e}$), or dielectric ($\boldsymbol{\varepsilon}^S$) properties. The variable ρ is a design variable describing the amount of material at each point of the domain, which can assume

values between 0 and 1, and N is the number of nodes in the finite element mesh.

Essentially, this material model approximates the material distribution by defining a function of a continuous parameter (design variable) that determines the mixture of basic materials throughout the domain. Regarding the numerical implementation, we consider the continuous distribution of the design variable within the finite element, which is interpolated by using the finite element shape functions.[24,25] In this case, the design variables are defined for each element node instead of each finite element as usual.

However, no design variable penalization is necessary in this case because the wave reflection is maximized when a wave encounters a defined interface where the material impedance mismatch is the greatest. As a result, 0–1 solutions naturally appear. The gray areas obtained in the final solution occur inside the elements that form the boundary between materials A and B because the design variables are defined at the nodes of the finite elements, and thus there is a continuous distribution of design variables inside these elements. As the numerical results presented in Sec. VI show, the optimized designs are rather insensitive with respect to gray areas. The corresponding design variables with intermediate values can be set to either 0 or 1 based on a chosen threshold value without noticeably changing of the wave performance.[16]

A. Projection method

A specific projection method is implemented in the unit-cell domain based on the approach developed by Carbonari *et al.*[26] that uses projection functions.[27] Nodes inside a circular region S_w^n in the neighborhood of the element of reference are included in the evaluation of the nodal design variables (ρ) used in the finite element analysis. The set of nodes S_w^n to be projected are defined by

$$\mathbf{x}_j \in S_w^n \text{ if } \mathrm{r_j^n} = |\mathbf{x_j} - \mathbf{x^n}| \leq \mathrm{r_{min}}, \tag{10}$$

where $\mathbf{x}_j$ are the coordinates of the node j, x^n are the coordinates of the node n, and r_j^e is the distance between the nodes n and j. The projection consists essentially of a cone of base $r_{\min}$ and unit height centered at the node n such that

$$\rho = \frac{\sum_{j \in S_w^n} d_j w(\mathbf{x}_j - \mathbf{x}^n)}{\sum_{j \in S_w^n} w(\mathbf{x}_j - \mathbf{x}^n)}, \tag{11}$$

$$w(\mathbf{x}_j - \mathbf{x}^n) = \max\left(\left(\frac{r_{grad} - r_j^n}{r_{grad}}\right)^q, 0\right). \tag{12}$$

The nodal variables d_j are weighted to evaluate the node volume fraction ρ_n of node n, as shown in Eq. (11), by using the weight function defined in Eq. (12). The coefficient q controls the penalization of the nodal values in the region Ω_w^n. Thus the problem relaxation is controlled through a constant r_{grad}, which is the radius of the linear projection function that covers the adjoining layers; and the penalization factor q, which controls the weight function in a non-linear way.[28] The optimization starts with $q = 1$ and its value is incremented by 1 at each of five iterations, until convergence of the objective function is achieved.

B. Topology optimization formulation

In this work, the adopted objective function aims to maximize the width of lower and higher order band gaps. The objective of the optimization is to maximize the difference between two adjacent eigenfrequencies ω_j and ω_{j+1}. This can be written as follows:[29]

$$\begin{aligned}
&\underset{d_i,\beta_1,\beta_2}{\text{Maximize:}} && F = \beta_2 - \beta_1 \\
&\text{subject to:} && [\mathbf{K}^*(\mathbf{k}) - \omega^2 \mathbf{M}^*]\,\mathbf{U}^* = \mathbf{0},\ \mathbf{k} \in [\Gamma \to \mathrm{X_1} \to \mathrm{M} \to \mathrm{X_2} \to \Gamma] \\
&&& \left[\omega_{j+1}^2(\mathbf{k})\right]_m \geq \beta_2,\ m = 1,\ldots,n_m \\
&&& \left[\omega_j^2(\mathbf{k})\right]_m \leq \beta_1 \\
&&& 0 \leq d_i \leq 1, \quad i = 1,\ldots,N \\
&&& \text{gradient control,}
\end{aligned} \tag{13}$$

where ω_j is the jth eigenfrequency in ascending order, m corresponds to the mth wavevector in the n_m-times discretized wavevector space, and β_1 and β_2 are independent design variables that act individually on the lower and upper constraint bounds, which locate the edges of the band gap. The sensitivities of this objective and set of constraints are presented in the next section. The value of the objective function can be negative, indicating that a band gap does not exist for the current design. The constraints, however, change with the design and their formulation does not require a pre-existing band gap, unlike other formulations.[30,31]

V. NUMERICAL IMPLEMENTATION

The numerical implementation is performed using MATLAB and verified with ANSYS via modal analysis. The

unit-cell is divided into 1600 bilinear quadrilateral elements (80×80 elements with 3 degrees of freedom at each node, two displacements, and one electric potential). The design variables are distributed in a 1/8 region of the unit cell, and the other parts are symmetric with respect to the design domain. Therefore the material distribution assumes a 1/8 symmetry, and the piezoelectric polarization is always in the vertical direction. Figure 2 shows an example of the design domain and the adopted symmetry condition.

The projection radius adopted is 5% of the unit cell length. After calculating the stiffness and mass matrices, the eigenvalues of Eq. (4) are computed for each reduced wave vector $\mathbf{k}$. During the implementation of this methodology, different initial material distributions (homogeneous, circular, circular graded, random) are tested, and a random initial guess with a volume fraction of 50% of piezoelectric material is selected to avoid local minima. Then the dispersion diagram is generated, and thus the band gap ranges can be measured. The sensitivity of the eigenvalues is calculated by differentiating Eq. (7) with respect to the design variables ρ_i, as follows:[32]

$$\frac{d\omega^2}{dd_i} = \sum_{j\in\Omega} \frac{d\omega^2}{d\rho_j}\frac{d\rho_j}{dd_i}, \tag{14}$$

$$\frac{d\omega^2}{d\rho_i} = \frac{\mathbf{U}_R^t\left(\frac{d\mathbf{K}_R}{d\rho_i} - \omega^2\frac{d\mathbf{M}_R}{d\rho_i}\right)\mathbf{U}_R}{\mathbf{U}_R^t\mathbf{M}_R\mathbf{U}_R}. \tag{15}$$

The maximization problem is solved through an iterative procedure, which is demonstrated in the flowchart of Fig. 3. After the iteration process converges, a specific post-processing procedure is performed to obtain a discrete topology. This is achieved by considering that all filtered density values above and below a threshold η are projected to 1 and 0, respectively. Then the dynamic analysis is performed again considering the post-processed result. The dispersion diagrams presented in the next section are obtained by using the post-processed material distribution. The optimization problem is solved by using the method of moving asymptotes (MMA) algorithm.[33]

VI. RESULTS AND DISCUSSIONS

This section explores the design of band gaps by using the topology optimization method. The materials adopted in this work are the PZT-5A piezoceramic and epoxy polymer the properties of which are listed in Table I.

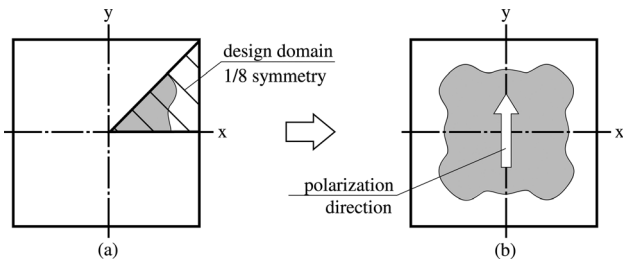

FIG. 2. Example of symmetry condition: (a) Design domain occupying 1/8 of the unit cell and (b) complete unit cell with symmetric parts, showing the polarization direction of piezoelectric material.

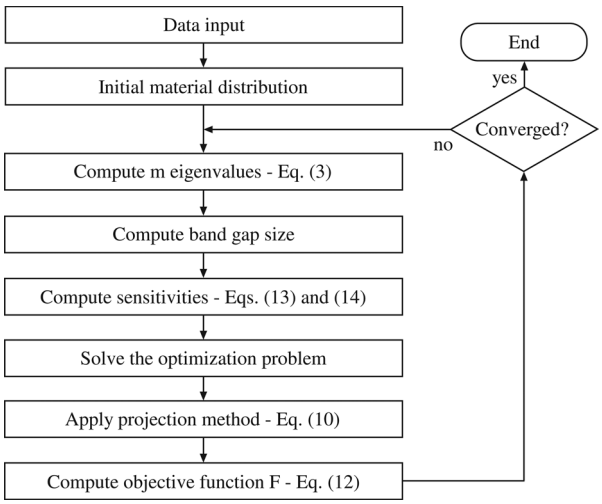

FIG. 3. Optimization problem flowchart.

To verify the influence of the piezoelectric effect in the dispersion diagram, the performance of a unit cell composed of PZT-5A cylinders embedded in epoxy is computed. The volume fraction of PZT-5A in the unit cell is 0.5. Two cases are performed, one with the piezoelectric properties presented in Table I and other with piezoelectric properties equal to zero. In the next figures, dark color indicates epoxy material and light color indicates PZT material. The dispersion diagrams for both cases are shown in Fig. 4, where it is possible to notice that the band gap width obtained with no piezoelectric properties ($\Delta\omega = 0.4283$) is smaller than that with piezoelectric properties ($\Delta\omega = 0.4916$), representing an increase in the band gap width of 15%. This example shows that the piezoelectric effect helps to improve the maximization of band gap widths. The transverse axis is the normalized frequency $\omega a_0/2\pi c_A$, where a_0 is the size of the unit cell, and c_A is the wave velocity of the material A, i.e., $\sqrt{E_A/\rho_A}$.

Optimized material designs are developed aiming at maximizing band gap widths of different orders, and the ten largest obtained gaps are presented. Not all the frequency bands could be obtained in this study, due to the symmetry imposed in the design domain. *The first band gap*, between the third and fourth branches, has a normalized band width equal to 0.5339 [see Fig. 5(a)], and the PZT-5A distribution

TABLE I. Material properties.

Property	PZT-5A	Epoxy
$c_{11}^E(10^{10}\ \mathrm{N/m^2})$	12.1	0.53
$c_{13}^E(10^{10}\ \mathrm{N/m^2})$	7.52	0.31
$c_{33}^E(10^{10}\ \mathrm{N/m^2})$	11.1	0.53
$c_{44}^E(10^{10}\ \mathrm{N/m^2})$	2.10	0.11
$e_{13}(\mathrm{C/m^2})$	−5.4	0
$e_{33}(\mathrm{C/m^2})$	15.8	0
$e_{15}(\mathrm{C/m^2})$	12.3	0
$\varepsilon_{11}^S/\varepsilon_0$	1650	4
$\varepsilon_{33}^S/\varepsilon_0$	1700	4

$\varepsilon_0 = 8.854188 \cdot 10^{-12} F/m$

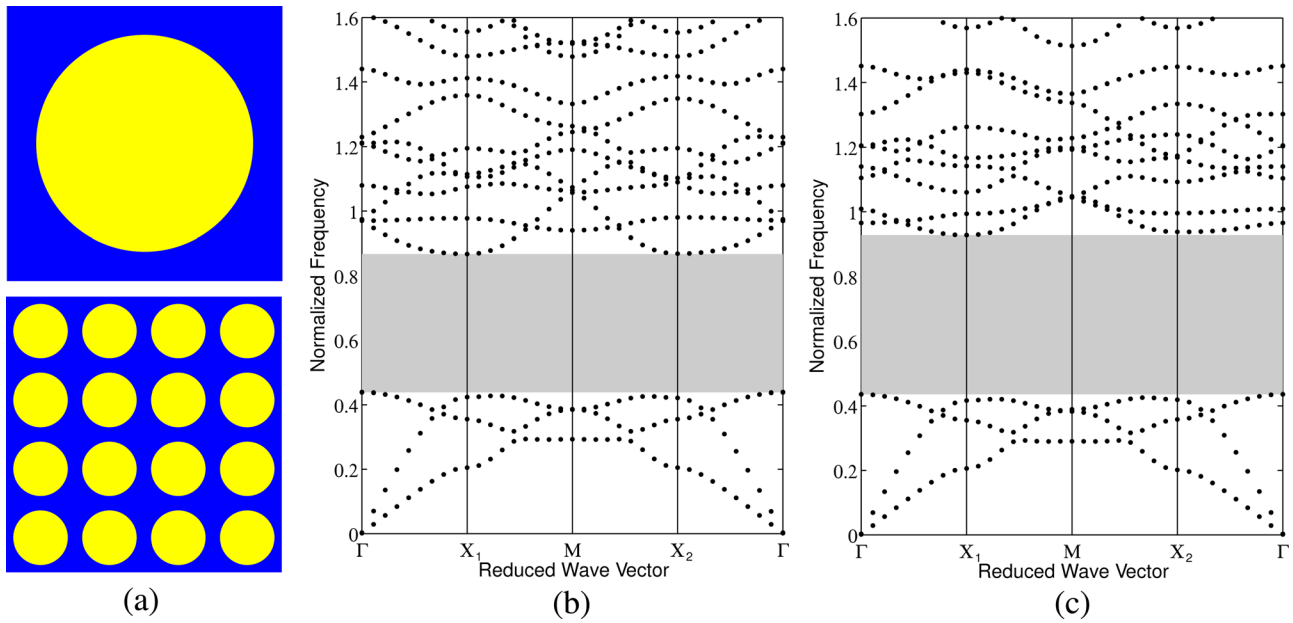

FIG. 4. (Color online) Influence of piezoelectric effect in a unit cell of PZT-5A cylinders embedded in epoxy: (a) Unit cell and periodic matrix, (b) dispersion diagram with no piezoelectric properties, and (c) with piezoelectric properties.

assumes an octagonal shape. Naturally, the final topology is formed by piezoelectric inclusions in an epoxy matrix.

The second band gap, between the 12th and 13th branches, has a normalized band width equal to 0.5548 [see Fig. 5(b)]. This gap is the biggest of all band gaps obtained for this combination of materials in this study. The concentration of PZT-5A in the middle of the unit cell, with an octagonal shape, is similar (however, not identical) to the unit cell obtained when the band gap between the third and fourth frequencies [Fig. 5(a)] is maximized. This example shows that the dispersion diagram is very sensitive to the scale effect of the topology. Notice that there is a multiscale effect in the unit cell design in the sense that the unit cell itself is recovered inside the design domain—see Fig. 5(b).

The third band gap, between the 13th and 14th branches, has a normalized band width equal to 0.0809 [see Fig. 6(a)]. In this case, there is another band gap located between the 17th and 18th frequencies with a normalized band width equal to 0.1250. However, this additional band gap is smaller than the one obtained when the objective function consists of enlarging this specific band gap (see following text).

The fourth band gap, between the 15th and 16th branches, has a normalized band width equal to 0.3266 [see Fig. 6(b)]. The topology obtained is formed by a concentration of PZT-5A in the middle of the unit cell with a "hole" of epoxy in its interior, and symmetric parts of PZT-5A around. *The fifth band gap*, between the 17th and 18th

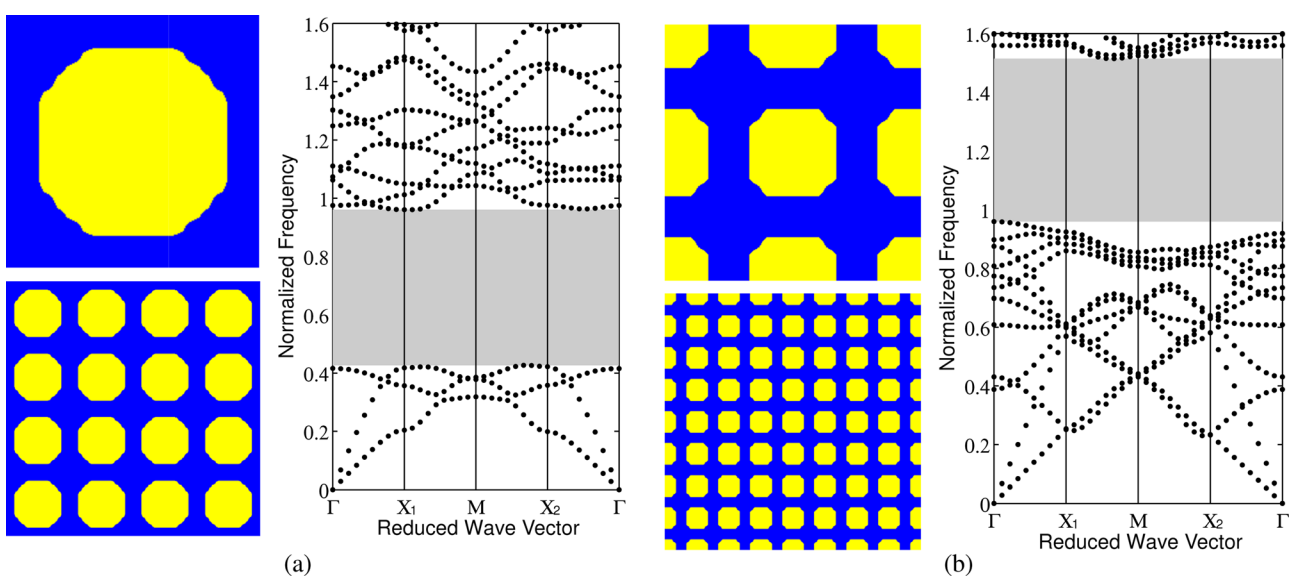

FIG. 5. (Color online) Unit cells, periodic matrices composed of four unit cells, and dispersion diagrams of the optimized results when maximizing the band gap between: (a) 3rd and 4th frequencies and (b) 12th and 13th frequencies.

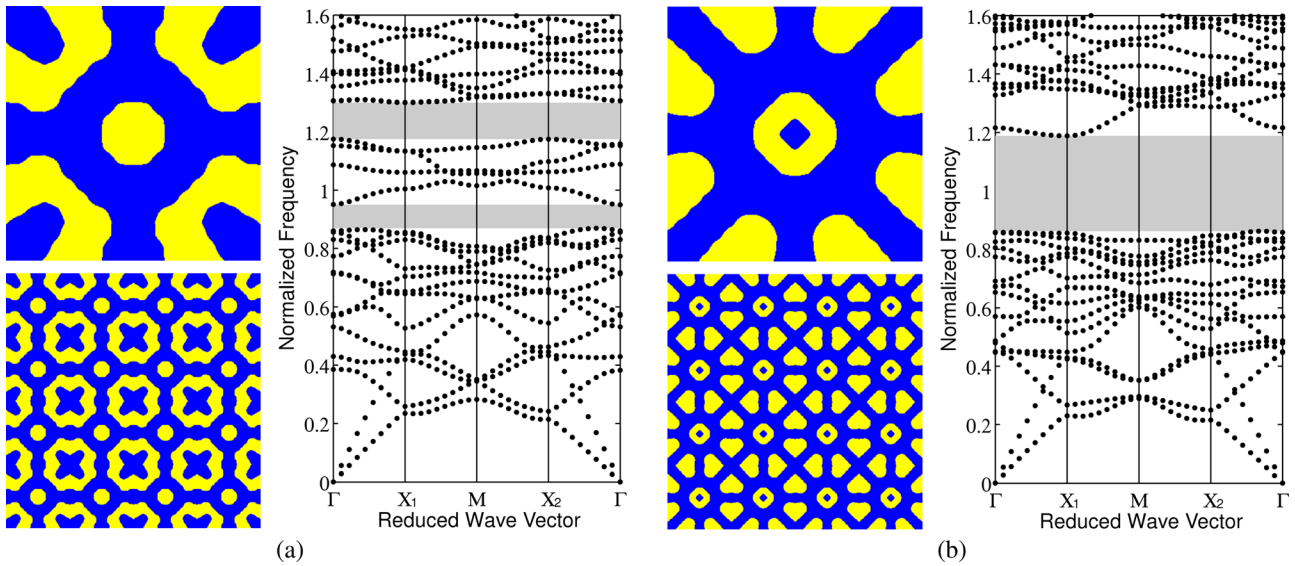

FIG. 6. (Color online) Unit cells, periodic matrices composed of four unit cells, and dispersion diagrams of the optimized results when maximizing the band gap between: (a) 13th and 14th frequencies and (b) 15th and 16th frequencies.

branches, has a normalized band width equal to 0.1614 [see Fig. 7(a)]. In this case, the topology is different from the last case, where there is a solid region of PZT-5A in the middle of the unit cell and hollowed shapes of epoxy. *The sixth band gap*, between the 24th and 25th branches, has a normalized band width equal to 0.3281 [see Fig. 7(b)], and the topology obtained is formed by solid regions of PZT-5A distributed in the epoxy.

VII. CONCLUDING REMARKS

In this work, a model for computing the propagation of plane acoustic waves in periodic materials has been applied to design piezocomposite materials. The main objective is to maximize the width of absolute elastic wave band gaps in piezocomposite materials designed using topology optimization. To that effect, finite element analysis is employed by considering the Bloch–Floquet theory to solve the dynamic behavior of two-dimensional piezocomposite unit cells. High order modes are investigated. All optimized topologies can be described as inclusions of PZT-5A in a soft matrix of epoxy. Due to symmetry imposed in the design domain, not all the frequency bands could be obtained in this study. The maximization of the first and second band gaps present similar optimized unit cells with different dispersion diagrams, showing that slight differences in the topology can affect the dispersion behavior of phononic materials. The maximization of the third band gap presents an unintentional band gap in the analyzed frequency range, while all the others presented only one band gap in the analyzed frequency range. However, this additional band gap is smaller than if it would be considered as the objective

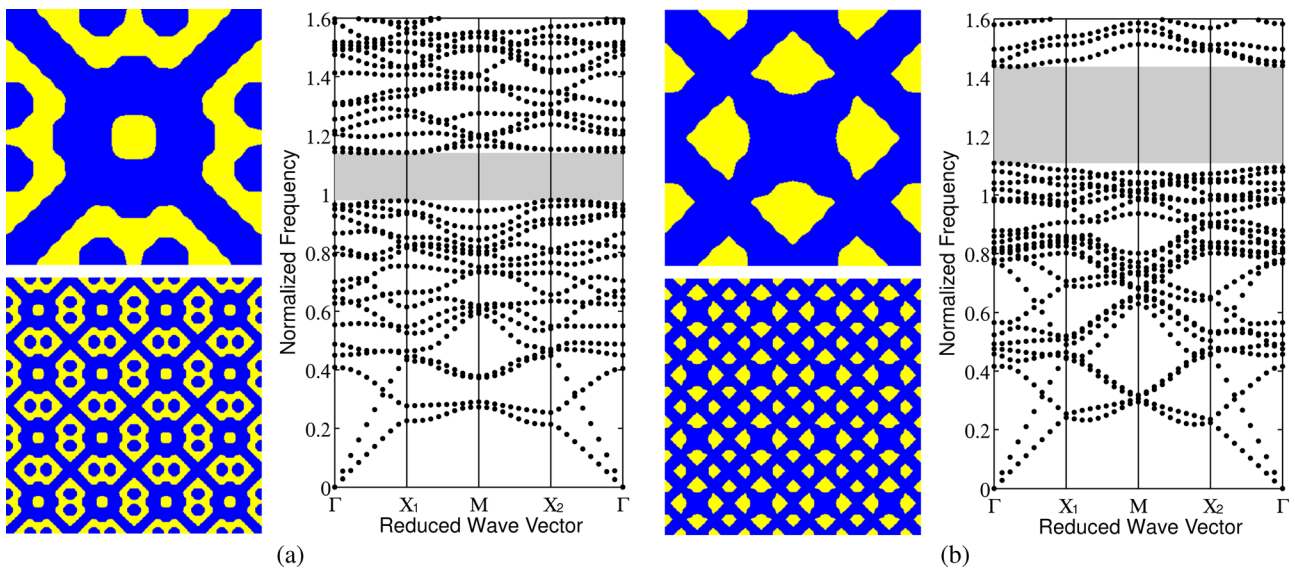

FIG. 7. (Color online) Unit cells, periodic matrices composed of four unit cells, and dispersion diagrams of the optimized results when maximizing the band gap between: (a) 17th and 18th frequencies and (b) 24th and 25th frequencies.

function target. Although the topologies presented in Fig. 5 are similar, the inclusions of PZT-5A on the second topology have half of the size of the first one. This difference in the size of the inclusions changes drastically the dispersion diagram of each case, showing the influence of the scale effect in the unit cell. The numerical examples presented in this work show that it is possible to design piezocomposite phononic materials aiming at maximizing band gaps for specific bands.

ACKNOWLEDGMENTS

The first author acknowledges FAPESP (São Paulo State Foundation Research Agency) for supporting him in his graduate studies through the Fellowship No. 2008/57086-6. The second author acknowledges support from the Donald and Elizabeth B. Willett endowment at the University of Illinois at Urbana-Champaign (UIUC). The third author thanks CNPq (National Council for Research and Development, Brazil) for Fellowship Nos. 304121/2013-4 and 562923/2008, and FAPESP research Project No. 2001/02387-4. The authors are grateful to Professor Svanberg for providing the source code for the Method of Moving Asymptotes (MMA).

[1]Z. H. Qian, F. Jin, Z. K. Wang, and K. Kishimoto, "Dispersion relations for SH-wave propagation in periodic piezoelectric composite layered structures," Int. J. Eng. Sci. **42**, 673–689 (2004).
[2]M. I. Hussein, K. Hamza, G. M. Hulbert, R. A. Scott, and K. Saitou, "Multiobjective evolutionary optimization of periodic layered materials for desired wave dispersion characteristics," Struct. Multidisciplinary Optim. **31**, 60–75 (2006).
[3]Y. Tanaka, Y. Tomoyasu, and S. Tamura, "Band structure of acoustic waves in phononic lattices: Two-dimensional composites with large acoustic mismatch," Phys. Rev. B **62**, 7387–7392 (2000).
[4]S. Gonella, A. C. To, and W. K. Liu, "Interplay between phononic bandgaps and piezoelectric microstructures for energy harvesting," J. Mech. Phys. Solids **57**, 621–633 (2009).
[5]O. Sigmund and J. S. Jensen, "Systematic design of phononic band-gap materials and structures by topology optimization," Philos. Trans. R. Soc. Lond. A Math. Phys. Eng. Sci. **361**, 1001–1019 (2003).
[6]M. L. Wu, L. Y. Wu, W. P. Yang, and L. W. Chen, "Elastic wave band gaps of one-dimensional phononic crystals with functionally graded materials," Smart Mater. Struct. **18**, 1–8 (2009).
[7]A. C. Hladkyhennion and J. N. Decarpigny, "Analysis of the scattering of a plane acoustic-wave by a doubly periodic structure using the finite-element method—Application to Alberich anechoic coatings," J. Acoust. Soc. Am. **90**, 3356–3367 (1991).
[8]R. Esquivelsirvent and G. H. Cocoletzi, "Band-structure for the propagation of elastic-waves in superlattices," J. Acoust. Soc. Am. **95**, 86–90 (1994).
[9]P. Langlet, A. C. Hladkyhennion, and J. N. Decarpigny, "Analysis of the propagation of plane acoustic-waves in passive periodic materials using the finite-element method," J. Acoust. Soc. Am. **98**, 2792–2800 (1995).
[10]R. James, S. M. Woodley, C. M. Dyer, and V. F. Humphrey, "Sonic bands, bandgaps, and defect states in layered structures—theory and experiment," J. Acoust. Soc. Am. **97**, 2041–2047 (1995).
[11]M. M. Sigalas, "Defect states of acoustic waves in a two-dimensional lattice of solid cylinders," J. Appl. Phys. **84**, 3026–3030 (1998).
[12]A. S. Phani, J. Woodhouse, and N. A. Fleck, "Wave propagation in two-dimensional periodic lattices," J. Acoust. Soc. Am. **119**, 1995–2005 (2006).
[13]M. Wilm, S. Ballandras, V. Laude, and T. Pastureaud, "A full 3D plane-wave-expansion model for 1-3 piezoelectric composite structures," J. Acoust. Soc. Am. **112**, 943–952 (2002).
[14]Z. L. Hou, F. G. Wu, and Y. Liu, "Phononic crystals containing piezoelectric material," Solid State Commun. **130**, 745–749 (2004).
[15]M. Wilm, A. Khelif, V. Laude, and S. Ballandras, "Design guidelines of 1-3 piezoelectric composites dedicated to ultrasound imaging transducers, based on frequency band-gap considerations," J. Acoust. Soc. Am. **122**, 786–793 (2007).
[16]M. P. Bendsoe and O. Sigmund, *Topology Optimization — Theory, Methods and Applications* (Springer, New York, 2003), 370 pp.
[17]O. Sigmund, "Topology optimization: A tool for the tailoring of structures and materials," Philos. Trans. R. Soc. A Math. Phys. Eng. Sci. **358**, 211–227 (2000).
[18]S. Halkjaer, O. Sigmund, and J. S. Jensen, "Inverse design of phononic crystals by topology optimization," Z. Kristallograph. **220**, 895–905 (2005).
[19]S. Halkjaer, O. Sigmund, and J. S. Jensen, "Maximizing band gaps in plate structures," Struct. Multidisciplinary Optim. **32**, 263–275 (2006).
[20]C. J. Rupp, A. Evgrafov, K. Maute, and M. L. Dunn, "Design of phononic materials/structures for surface wave devices using topology optimization," Struct. Multidisciplinary Optim. **34**, 111–121 (2007).
[21]ANSI S176-1987: "An American National Standard–IEEE standard on piezoelectricity," IEEE Trans. Sonics Ultrason. **31**, 1–55 (1984).
[22]T. Ikeda, *Fundamentals of Piezoelectricity* (Oxford University Press, Oxford, UK, 1996), 280 pp.
[23]M. Naillon, R. H. Coursant, and F. Besnier, "Analysis of piezoelectric structures by a finite-element method," Acta Electron. **25**, 341–362 (1983).
[24]J. H. Kim and G. H. Paulino, "Isoparametric graded finite elements for nonhomogeneous isotropic and orthotropic materials," ASME J. Appl. Mechan. **69**, 502–514 (2002).
[25]K. Matsui and K. Terada, "Continuous approximation of material distribution for topology optimization," Int. J. Num. Methods Eng. **59**, 1925–1944 (2004).
[26]R. C. Carbonari, E. C. N. Silva, and G. H. Paulino, "Topology optimization design of functionally graded bimorph-type piezoelectric actuators," Smart Mater. Struct. **16**, 2607–2620 (2007).
[27]J. K. Guest, J. H. Prévost, and T. Belytschko, "Achieving minimum length scale in topology optimization using nodal design variables and projection functions," Int. J. Num. Methods Eng. **61**, 238–254 (2004).
[28]S. R. M. Almeida, G. H. Paulino, and E. C. N. Silva, "A simple and effective inverse projection scheme for void distribution control in topology optimization," Struct. Multidisciplinary Optim. **39**, 359–371 (2009).
[29]C. J. Rupp, "Topology optimization for wave propagation and vibration phenomena in elastic and piezoelectric," Ph.D. thesis, Department of Mechanical Engineering, University of Colorado, 2009.
[30]S. J. Cox and D. C. Dobson, "Maximizing band gaps in two-dimensional photonic crystals," SIAM J. Appl. Math. **59**, 2108–2120 (1999).
[31]S. J. Cox and D. C. Dobson, "Band structure optimization of two-dimensional photonic crystals in h-polarization," J. Comput. Phys. **158**, 214–224 (2000).
[32]E. C. N. Silva and N. Kikuchi, "Design of piezocomposite materials and piezoelectric transducers using topology optimization. Part III," Arch. Comput. Methods Eng. **6**, 305–329 (1999).
[33]K. Svanberg, "The method of moving asymptotes—A new method for structural optimization," Int. J. Num. Methods Eng. **24**, 359–373 (1987).